

A graphical analysis of the systematic error of classical binned methods in constructing luminosity functions

Zunli Yuan^{1,2,3} • Jiancheng Wang^{1,2}

Abstract The classical $1/V_a$ and PC methods of constructing binned luminosity functions (LFs) are revisited and compared by graphical analysis. Using both theoretical analysis and illustration with an example, we show why the two methods give different results for the bins which are crossed by the flux limit curves $L = L_{lim}(z)$. Based on a combined sample simulated by a Monte Carlo method, the estimate ϕ of two methods are compared with the input model LFs. The two methods give identical and ideal estimate for the high luminosity points of each redshift interval. However, for the low luminosity bins of all the redshift intervals both methods give smaller estimate than the input model. We conclude that once the LF is evolving with redshift, the classical binned methods will unlikely give an ideal estimate over the total luminosity range. Page & Carrera (2000) noticed that for objects close to the flux limit ϕ_{1/V_a} nearly always to be too small. We believe this is due to the arbitrary choosing of redshift and luminosity intervals. Because ϕ_{1/V_a} is more sensitive to how the binning are chosen than ϕ_{PC} . We suggest a new binning method, which can improve the LFs produced by the $1/V_a$ method significantly, and also improve the LFs produced by the PC methods. Our simulations show that after adopting this new binning, both the $1/V_a$ and PC methods have comparable results.

Keywords galaxies: luminosity function, mass function — galaxies: quasars: general

Zunli Yuan

Jiancheng Wang

Email: yuanzunli@ynao.ac.cn

¹National Astronomical Observatories, Yunnan Observatory, Chinese Academy of Sciences, Kunming 650011, China.

²Key Laboratory for the Structure and Evolution of Celestial Objects, Chinese Academy of Sciences, Kunming 650011, China.

³Graduate School, Chinese Academy of Sciences, Beijing, China.

1 Introduction

From shortly after the first quasar was found until the present, considerable effort has been spent in obtaining samples to investigate their luminosity distribution as a function of redshift, known as the luminosity function (LF). The LF is very important because its shape and evolution provide constraints on the nature of activity and the cosmic evolution of quasars/active galactic nuclei (AGNs). Up to now many statistical approaches have been proposed to investigate the LFs. These include parametric techniques which assume analytical form for the LFs, and non-parametric methods which usually need binning the data (see Johnston 2011, for an overall review).

Among the non-parametric methods, the $1/V_a$ estimator (see Avni & Bahcall 1980; Eales 1993; Ellis et al. 1996) is the most classical binned method and is particularly prevalent for its simplicity. Although more than four decades have passed since its original version (i.e., the famous $1/V_{max}$ estimator, Schmidt 1968) was presented, the $1/V_a$ method is not outdated and continues to be widely used in the literature (see Civano et al. 2011; Mao et al. 2012; Marchesini et al. 2012; McAlpine & Jarvis 2011; Padovani et al. 2011; Patel et al. 2012; Hiroi et al. 2012; Yuan & Wang 2012; Marchã & Caccianiga 2013, for latest use). On the other hand, authors have pointed out that the $1/V_a$ method introduces a significant error for objects close to the flux limit (e.g., Page & Carrera 2000; Cara & Lister 2008). Page & Carrera (2000) presented an improved method (hereafter the PC method) of constructing the binned LF. According to the result based on a Monte Carlo simulation, the authors believed their method is superior to the $1/V_a$ method in many aspects. However, their simulation was performed using a luminosity function which is unchanging with redshift (i.e. no evolution) and a single flux limit. The assumption of no

evolution is too particular to be able to represent more general situations. Furthermore, they focused on the situation of single sample (a single flux limit), and the discussion on multiple samples was not sufficient. In this paper, we revisit the $1/V_a$ and PC methods to find the reason of systematic error using graphical analysis. The situation when multiple samples are combined to obtain a LF is particularly discussed. By the way, in recent years some more sophisticated and rigorous methods have emerged (e.g., Schafer 2007; Kelly et al. 2008; Christlein et al. 2009; Takeuchi 2010; Johnston et al. 2012). Nevertheless, it needs time for the new methods to be recognized and in widespread use. During this time, specifying deficiencies of the old methods could be helpful.

Throughout the paper, we adopt a Lambda Cold Dark Matter cosmology with the parameters $\Omega_m = 0.27$, $\Omega_\Lambda = 0.73$, and $H_0 = 71 \text{ km s}^{-1} \text{ Mpc}^{-1}$.

2 Methods

The differential LF $\phi(L, z)$ is defined as the number density of target sources per unit comoving volume per unit luminosity interval, i.e.

$$\phi(L, z) = \frac{d^2N}{dVdL}(L, z). \quad (1)$$

More often it is defined in terms of $\log L$. In this paper we do not differentiate L and $\log L$ strictly.

2.1 The $1/V_a$ method

The $1/V_a$ method originates from the celebrated paper by Avni & Bahcall (1980), which generalized V/V_{max} (Schmidt 1968) for multiple samples. Here we consider two flux-limited samples observed at the same frequencies. For simplicity, we assume the two samples to be not overlapping in survey regions, as shown in Fig. 1. Sample D (D denotes deep) is assumed to be deeper in all the sample frequencies than Sample B (B denotes bright). Let S_{lim}^D and S_{lim}^B denote their flux limits respectively, then $S_{lim}^D < S_{lim}^B$.

If N objects appear in the interval $\Delta L \Delta z$ ($L_1 < L < L_2, z_1 < z < z_2$) around the bin center (L, z) , the LF is estimated as

$$\phi_{1/V_a}(L, z) = \frac{1}{\Delta L} \sum_{i=1}^N \frac{1}{V_a^i}. \quad (2)$$

According to the scenario of Avni & Bahcall (1980), the sample B and D can be combined into a ‘‘coherent sample’’. It can be regarded as a single sample, in which

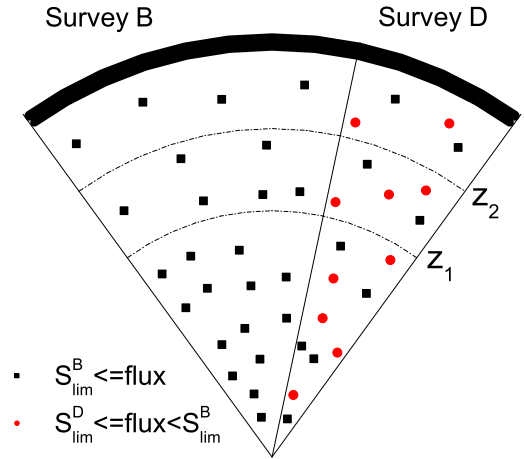


Fig. 1 Sample B and D. All data points are simulated. Sample D is assumed to be deeper in all frequencies than Sample B. Let S_{lim}^D and S_{lim}^B denote their flux limits respectively, then $S_{lim}^D < S_{lim}^B$. The red solid circles represent objects with fluxes between S_{lim}^D and S_{lim}^B , while the black solid squares represent those with fluxes above S_{lim}^B .

each object is allowed to be distributed anywhere within the total volume. Thus the available volume V_a for any object i in sample B and D can be calculated as

$$V_a^i = \sum_{S=B,D} \Omega_S(z_1, z_{max}^{iS}) \int_{z_1}^{z_{top}^{iS}} \frac{dV}{dz} dz, \quad (3)$$

where $\Omega_S(z_1, z_{max}^{iS})$ is the effective survey area in steradians of the S th survey. We have $\Omega_S(z_1 < z_{max}^{iS}) = \Omega_S$ and $\Omega_S(z_1 \geq z_{max}^{iS}) = 0$. Ω_B and Ω_D are the solid angles subtended by B and D samples on the sky respectively. z_{top}^{iS} is defined as

$$z_{top}^{iS} = \min[z_2, z_{max}^{iS}] = \min[z_2, z(L_i, S_{lim}^S)], \quad (4)$$

However, one must keep in mind that the sources with fluxes between S_{lim}^D and S_{lim}^B (represented by red solid circles in Fig. 1, hereafter red sources) can never appear in sample B. In the $L - z$ plane (shown in Fig. 2), these sources are located between the curves $L = L_{lim}^B(z)$ and $L = L_{lim}^D(z)$, which represent the flux limits of survey B and D respectively. On the other hand the sources with fluxes above S_{lim}^B (represented by black solid squares in Fig. 1, hereafter black sources) may appear both in sample B and D. The above discussion helps us to distinguish the actual surveyed regions corresponding to red and black sources.

2.2 The PC method

The key point of the $1/V_a$ method is that it takes into account the contribution of object i to the number den-

sity of the bin $\Delta L \Delta z$ as $1/(\Delta L V_a^i)$. Page & Carrera (2000) presented an improved method of constructing the binned LF (also see Tzanavaris & Georgantopoulos 2008; Yenko et al. 2009). That is, the LF at the center of a bin with a luminosity interval L_1 and L_2 and a redshift interval z_1 and z_2 can be estimated as

$$\phi_{PC} = \frac{N}{\int_{L_1}^{L_2} \int_{z_1}^{z_{max}(L)} \frac{dV}{dz} dz dL} \quad (5)$$

where N is the number of sources detected within the bin, and the double integral corresponds to the shaded area of bin 1 in Fig. 2. The key point of the *PC* method is to consider the actual surveyed region of a bin as a four-dimensional polyhedron in the volume-luminosity space, and the ϕ_{PC} for this bin is the four-number-density.

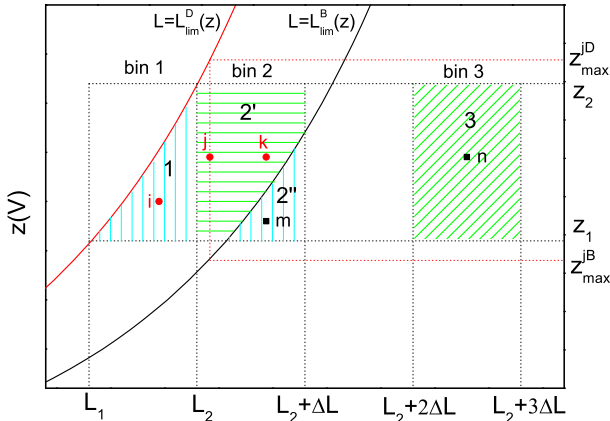


Fig. 2 L - z plane for the simulated sources from sample B and D. Only a part of the sources are plotted. The black solid line $L = L_{lim}^B(z)$ is the flux limit curve of sample B, and similarly for $L = L_{lim}^D(z)$. The shaded regions marked by 1, 2', 2'' and 3 represent the surveyed regions of bin 1, bin 2 and bin 3. A few example sources with different locations and status, i.e. i, j, k, m , and n , are shown in red and black dots. The red dotted lines are auxiliary lines to illustrate the values of z_{max}^{jB} and z_{max}^{iD} .

2.3 Comparison of the two methods

Here we take into account three situations represented by bin 1, bin 2, bin 3 in Fig. 2. For them, the shaded regions are the regions of the volume-luminosity plane in the interval $\Delta L \Delta z$ that has been surveyed (also see Page & Carrera 2000), and are marked by 1, 2', 2'' and 3. For bin 2, because either red or black sources appear

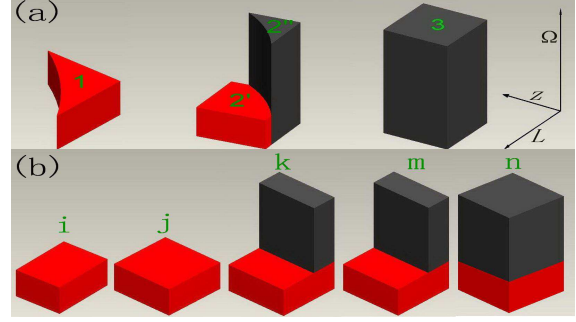


Fig. 3 Illustration of the surveyed regions and the area equal to $[\Delta L V_a]$. (a) illustrates the surveyed regions of bin 1, bin 2 and bin 3. (b) illustrates the area equal to $[\Delta L V_a^i]$, $[\Delta L V_a^j]$, $[\Delta L V_a^k]$, $[\Delta L V_a^m]$ and $[\Delta L V_a^n]$ of the example sources i, j, k, m and n respectively.

in it, 2' and 2'' are used to represent different surveyed regions. In the volume-luminosity space, these shaded regions are four-dimensional polyhedrons illustrated in Fig. 3(a). Their four-volumes can be calculated as

$$A_1 = \Omega_D \int_{L_1}^{L_2} \int_{z_1}^{z_{max}^D(L)} \frac{dV}{dz} dz dL. \quad (6)$$

$$A_{2'} = \Omega_D \int_{L_2}^{L_2+\Delta L} \int_{z_{max}^B(L)}^{z_2} \frac{dV}{dz} dz dL. \quad (7)$$

$$A_{2''} = (\Omega_D + \Omega_B) \int_{L_2}^{L_2+\Delta L} \int_{z_1}^{z_{max}^B(L)} \frac{dV}{dz} dz dL. \quad (8)$$

$$A_3 = (\Omega_D + \Omega_B) \int_{L_2+2\Delta L}^{L_2+3\Delta L} \int_{z_1}^{z_2} \frac{dV}{dz} dz dL. \quad (9)$$

Therefore, according to section 2.2, the estimated LF by the *PC* method ϕ_{PC} for bin 1, bin 2 and bin 3 are calculated as N_1/A_1 , $N_2/(A_{2'} + A_{2''})$ and N_3/A_3 , where N_1 , N_2 and N_3 are the numbers of sources detected within bin 1, bin 2 and bin 3, and A_1 , $A_{2'}$, $A_{2''}$ and A_3 are defined by Eq.(5)-(8). It is emphasized that N_2 is the sum of red and black sources detected within bin 2.

In the use of the $1/V_a$ method, the available volume V_a of every source should be calculated. The calculation of V_a for a source depends on its location in a bin. In Fig.2, a few example sources with different locations and status are labeled as i, j, k, m , and n respectively.

1. bin 1: Only red sources can appear in the bin. For a source i (represented by the red solid circle labeled 'i' in Fig. 2) in bin 1, as $z_{max}^{iB} < z_1$, we have

$$V_a^i = \Omega_D \int_{z_1}^{z_{max}^{iD}} \frac{dV}{dz} dz. \quad (10)$$

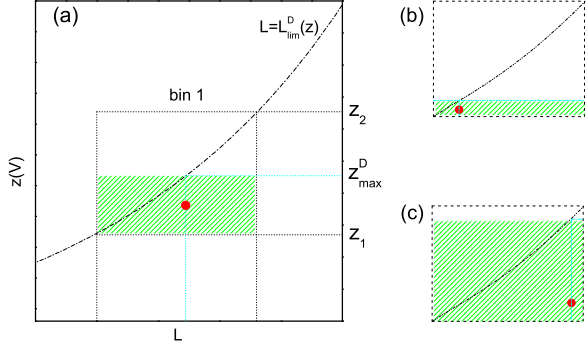


Fig. 4 Available volume V_a^i for an object i within bin 1. The area equal to $[\Delta LV_a^i]$ is indicated by the shaded region in (a). It is noticed that this area depend on the position of object i within bin 1. (b) and (c) show how this area changes dramatically in two extreme situations when an object i is located at the left and right margin respectively within the bin.

The area equal to $[\Delta LV_a^i]$ for an object i (represented by a red spot) is shown in Fig. 4(a). This area is clearly not the same as that of the surveyed region (the shaded region of bin 1, marked as 1 in Fig. 2). The deviation depends on the position of an object i in bin 1. If the object locates at the left margin of bin 1 (see Fig. 4(b)), the area equal to $[\Delta LV_a^i]$ (the shaded region in Fig. 4(b)) will be much smaller than that of the surveyed region (the shaded region of bin 1, in Fig. 2), and vice versa (see Fig. 4(c)). Hence ϕ_{1/V_a} and ϕ_{PC} will give different estimates of ϕ for this bin.

2. bin 2: Both red and black sources appear in the bin. However they belong to different surveyed regions (represented by $2'$ and $2''$ respectively). For a source j (represented by the red solid circle labeled 'j' in Fig. 2) in bin 2, when $z_{max}^{jB} < z_1$ and $z_2 < z_{max}^{jD}$, we have

$$V_a^j = \Omega_D \int_{z_1}^{z_2} \frac{dV}{dz} dz. \quad (11)$$

For a source k (represented by the red solid circle labeled 'k' in Fig. 2) in bin 2, when $z_1 < z_{max}^{kB} < z_2$ and $z_2 < z_{max}^{kD}$, we have

$$V_a^k = \Omega_B \int_{z_1}^{z_{max}^{kB}} \frac{dV}{dz} dz + \Omega_D \int_{z_1}^{z_2} \frac{dV}{dz} dz. \quad (12)$$

Although source m (represented by the black square labeled 'm' in Fig. 2) is a black one, its situation is

similar to source k with

$$V_a^m = \Omega_B \int_{z_1}^{z_{max}^{mB}} \frac{dV}{dz} dz + \Omega_D \int_{z_1}^{z_2} \frac{dV}{dz} dz. \quad (13)$$

The total surveyed region of bin 2 is the sum of $2'$ and $2''$. The area equal to $[\Delta LV_a^j]$ (see Fig. 3(b), j specifically) is clearly smaller than that of the surveyed region (Fig. 3(a), $2' + 2''$). Consequently, the density contribution of a source like j to bin 2 is positive, and possibly leads ϕ_{1/V_a} to give a exaggerated estimate for bin 2. The area equal to $[\Delta LV_a^k]$ as well as $[\Delta LV_a^m]$ are approximations of the surveyed region of bin 2. Overall, ϕ_{1/V_a} possibly gives a higher estimate of ϕ than ϕ_{PC} for this bin.

3. bin 3: Only black sources appear in the bin. For a source n (represented by the black square labeled 'n' in Fig. 2) in bin 3, as $z_2 < z_{max}^{nB} < z_{max}^{nD}$, we have

$$V_a^n = \Omega_B \int_{z_1}^{z_2} \frac{dV}{dz} dz + \Omega_D \int_{z_1}^{z_2} \frac{dV}{dz} dz. \quad (14)$$

The area equal to $[\Delta LV_a^n]$ for an object n is the same as that of the surveyed region and hence ϕ_{1/V_a} and ϕ_{PC} will give the same estimate of ϕ for this bin.

To sum up, the two methods give different results for the bins which are crossed by the flux limit curves $L = L_{lim}(z)$.

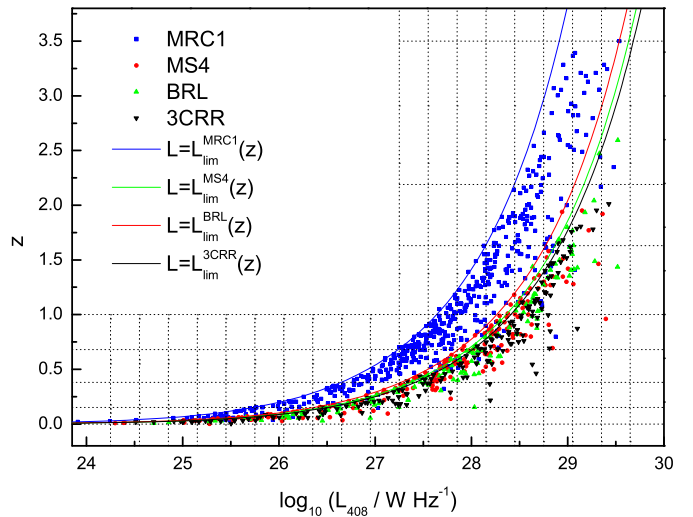


Fig. 5 $L-z$ plane of the sources from the combined sample established by Yuan & Wang (2012). The sample consists of four surveys, each represented by different symbols. When these data points are binned to use the $1/V_a$ or PC methods, much more bins are crossed by the flux limit curves $L = L_{lim}(z)$.

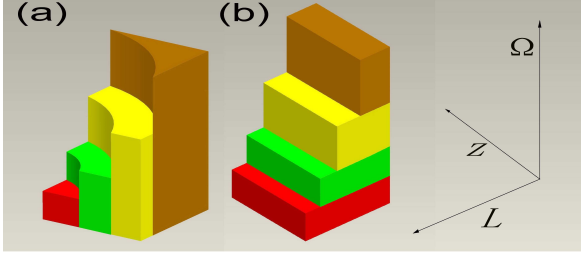


Fig. 6 This is an example bin of combined sample from more than two samples. It is divided into multi-regions by the flux limit curves. (a) and (b) illustrate the surveyed regions and the area equal to $[\Delta LV_a^i]$ respectively.

2.4 Multiple Samples

Practically many samples with different depth, extent and degrees of completeness are combined to obtain a LF that spans a wide range of luminosities and redshifts. When the sources from different samples are plotted on the redshift-luminosity plane and binned to use the $1/V_a$ or PC methods, much more bins are crossed by one or more flux limit curves. Some bins are divided into multiple regions by the flux limit curves $L = L_{lim}(z)$ (see Fig. 5 for an example). In this case, the area equal to $[\Delta LV_a^i]$ for an object i is a gross approximation to that of the surveyed region (see Fig. 6). ϕ_{PC} and ϕ_{1/V_a} will give different estimate of ϕ for these bins.

2.5 Applying the methods to real data

In this section we apply the $1/V_a$ and PC methods to the combined sample established by Yuan & Wang (2012). Fig. 5 shows the $L - z$ plane of the combined sample. The four sub-samples, MRC1 (McCarthy et al. 1996), MS4 (Burgess & Hunstead 2006), BRL (Best et al. 1999) and 3CRR (Laing et al. 1983) are described in the paper of Yuan & Wang (2012). For comparison, the radio luminosity function (RLF) at 408 MHz estimated by the two methods are plotted together for all the redshift bins in Fig. 7. It is not surprising that the two methods give the same results at the bright end of the RLFs, corresponding to the situation of bin 3 discussed in section 2.3. It is clear that ϕ_{1/V_a} and ϕ_{PC} give different estimates at the faint end and middle of the RLFs. ϕ_{1/V_a} trends to give a smaller estimate than ϕ_{PC} at the faint end, while it gives a larger estimate in the middle of the RLFs. Especially for the high redshift bins, ϕ_{1/V_a} gives a significantly larger estimate than ϕ_{PC} in the middle of the RLFs. Because the situation like that for source j in bin 2 (discussed in section 2.3) is more prevalent for high redshift bins.

2.6 Monte Carlo simulation

In this section we use a combined sample simulated by a Monte Carlo method to further compare the $1/V_a$ and PC methods. The simulation is performed using a double-power-law model radio luminosity function which is changing with redshift in the form of $(1+z)^k$. The Monte Carlo simulation produces four flux-limited samples containing more than 1 000 000 sources. The flux limits of the four simulated samples are 0.6 Jy, 1.2 Jy, 2.2 Jy, and 3.0 Jy respectively, and the solid angles subtended by them are 0.6 Sr, 1.2 Sr, 2.2 Sr and 3.0 Sr respectively. Without loss reality, a random spectral index following a normal distribution with an average of 0.7 is arranged for all the simulated sources. The four simulated samples are then combined into a “coherent sample” and binned LFs are produced for it in a range of redshift intervals using both methods. These are shown in Fig. 8, ϕ_{1/V_a} on the left and ϕ_{PC} on the right. The input model LFs take values of $z = 0.12, 0.35, 0.75, 1.25, 1.75, 2.25$ and are shown as dashed lines.

As expected from section 2.3, the two methods give identical and ideal estimate for the high luminosity points of each redshift interval. However, for the low luminosity bins of all the redshift intervals both methods give smaller estimate than the input model. This situation is especially serious for the $1/V_a$ method. For the lowest luminosity bins of the $1.0 < z < 1.5, 1.5 < z < 2.0, 2.0 < z < 2.5$ redshift intervals ϕ_{1/V_a} is significantly smaller than the input model.

The above results are not in completely agreement with Page & Carrera (2000). Their simulation showed that ϕ_{PC} is always a good representation of the input model over the total luminosity range. This is because their simulation was performed using a LF which is unchanging with redshift (i.e. no evolution). Once the LF is evolving with redshift, the classical binned methods will unlikely give an ideal estimate over the total luminosity range. In Fig. 9 we show how this happens.

In Fig.9 (a), bin1,bin2,bin3 are three bins located at different luminosity. Each bin is further divided into nine sub-bins. We assume each sub-bin is small enough and the four-volume involved is unit. The number noted in each sub-bin represents the source number. Thus the variation of number across sub-bins indicates how the density changes along luminosity and redshift. According to the PC method, the density (i.e., LF) at the center of bin2 and bin3 is estimated as 10 and 4 respectively. This is in agreement with the input model density at z_{mid} (see Fig.9 (b)). Bin1 is divided into two parts by the flux limit curve $L = L_{lim}(z)$. Owing to the positive evolution of density along redshift and decline

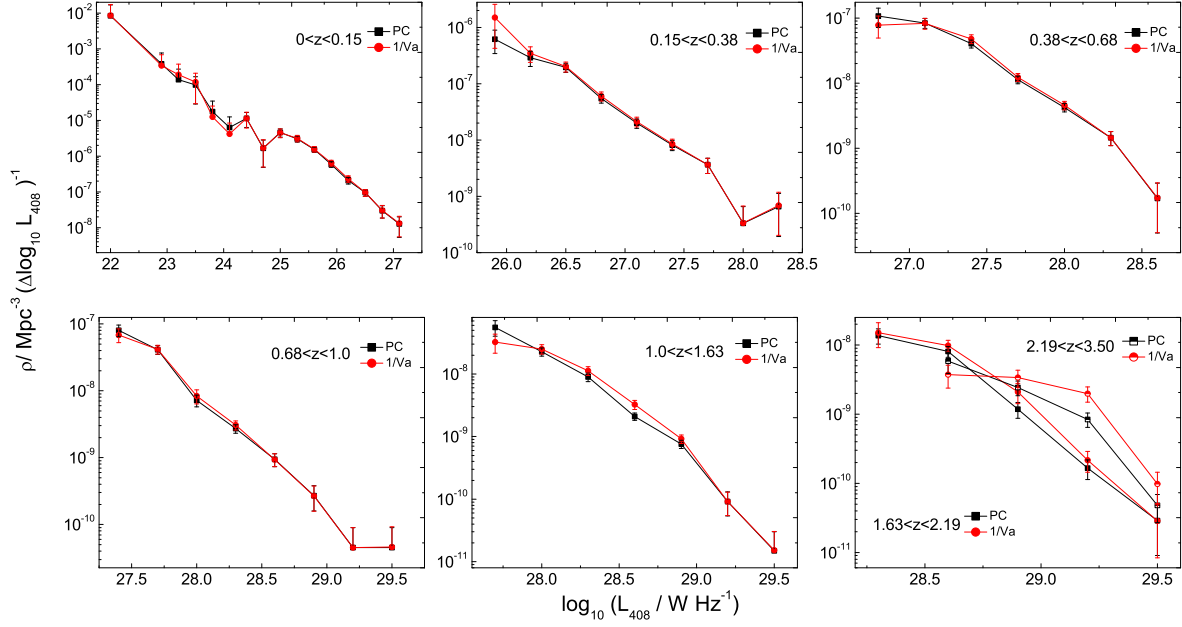


Fig. 7 Comparison of the RLFs at 408 MHz estimated by the binned $1/V_a$ and PC methods are plotted together for all redshift bins. The two methods give same results at the bright end of the LFs, but they give different estimates at the faint end and middle of the RLFs.

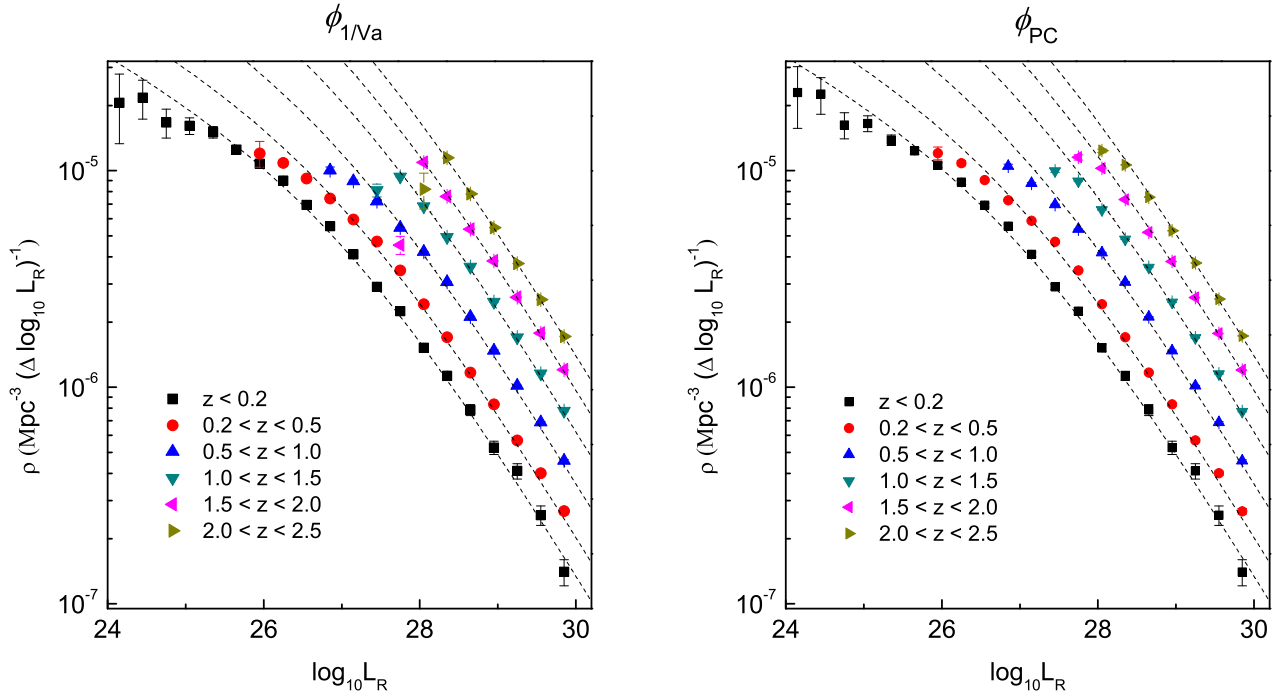


Fig. 8 Binned luminosity functions of simulated samples of objects using (left) ϕ_{1/V_a} and (right) ϕ_{PC} . The input model LFs take values of $z = 0.12, 0.35, 0.75, 1.25, 1.75, 2.25$ and are shown as dashed lines.

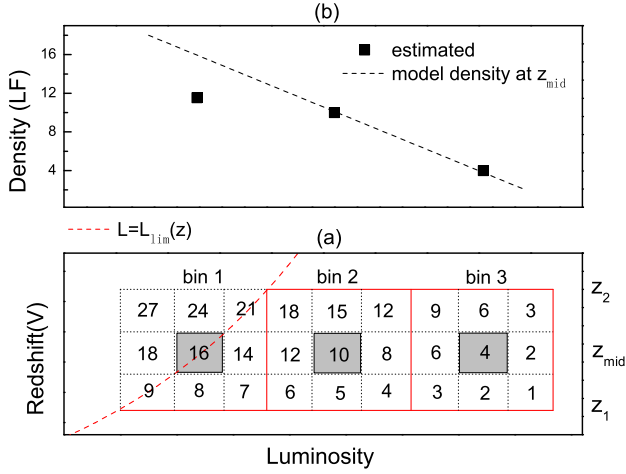


Fig. 9 This figure show that as long as the LF is evolving with redshift, the classical binned methods will unlikely give an ideal estimate over the total luminosity range. (a): bin1,bin2,bin3 are three bins located at different luminosity. Each bin is further divided into nine sub-bins. Each sub-bin is assumed to be small enough and the four-volume involved is unit. The number noted in each sub-bin represents the source number. Thus the variation of number across sub-bins indicates how the density changes along luminosity and redshift. (b): The model density (LF) at z_{mid} is shown as black dashed lines. The estimated density of the three bins by the *PC* method are shown as black dots.

of density along luminosity, the left part of bin1 probably contains more sources than the right part. However, the sources in left part can not be observed because the flux is limited. Therefore, according to the *PC* method, the density at the center of bin1 is estimated as 10.55 (the total source number in right part of bin1 divided by its four-volume) which is significantly smaller than the input model density. It can be expected that the more intensely the LF evolves with redshift, the more significant the error of ϕ_{PC} for bin1 is. The above discussion also applies to the $1/V_a$ method.

2.7 A simple rule of thumb to determine the redshift and luminosity intervals

The accuracy of binned LF also depends on how the redshift and luminosity bins are divided. The bins are supposed to be small enough, but can not be too small to include only a few objects. In general, the equal intervals of luminosity are used, e.g. $\Delta L = 0.3$ or 0.5 . While in the literature, the redshift intervals are commonly chosen something arbitrarily, e.g. $0.0 < z < 0.2$, $0.2 < z < 0.5$, $0.5 < z < 1.0$; $0.0 < z < 0.15$, $0.15 < z < 0.4$, $0.4 < z < 0.7$ etc. We believe this may lead the bins located at the faint end to enclose

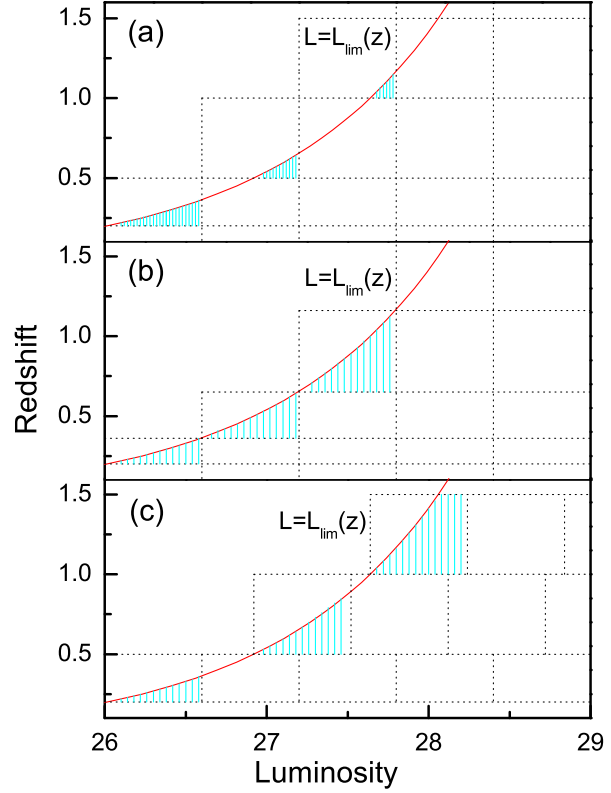


Fig. 10 Determination of the redshift and luminosity bins. (a): The redshift intervals are chosen arbitrarily. (b): The redshift intervals are determined by the intersecting points of luminosity grid-line and flux limit curve. (c): The luminosity intervals are determined by the intersecting points of redshift grid-line and flux limit curve. The shaded regions represent the surveyed regions. The surveyed regions only occupy very small parts of the faint end bins in (a), this probably lead them to enclose very few objects which gather at the right margins. This issue is avoided in (b) and (c).

very few objects inside(see Fig. 10 (a)) and cause bias with small number statistics. Moreover, in these bins, objects necessarily gather at the right margins (see Fig. 4(c)). Thus the area equal to $[\Delta LV_a]$ of these bins will be much larger than that of the surveyed regions, causing a significantly small estimate of ϕ_{1/V_a} . To tackle this issue, we take the redshift intervals to be determined by the intersecting points of luminosity grid-line and flux limit curve (see Fig. 10 (b)). Alternatively, if one persists in dividing redshift intervals randomly, the luminosity intervals should be determined by the intersecting points of redshift grid-line and flux limit curve (see Fig. 10 (c)).

Fig. 11 shows the binned LFs produced by the $1/V_a$ and *PC* methods for our simulated data with the red-

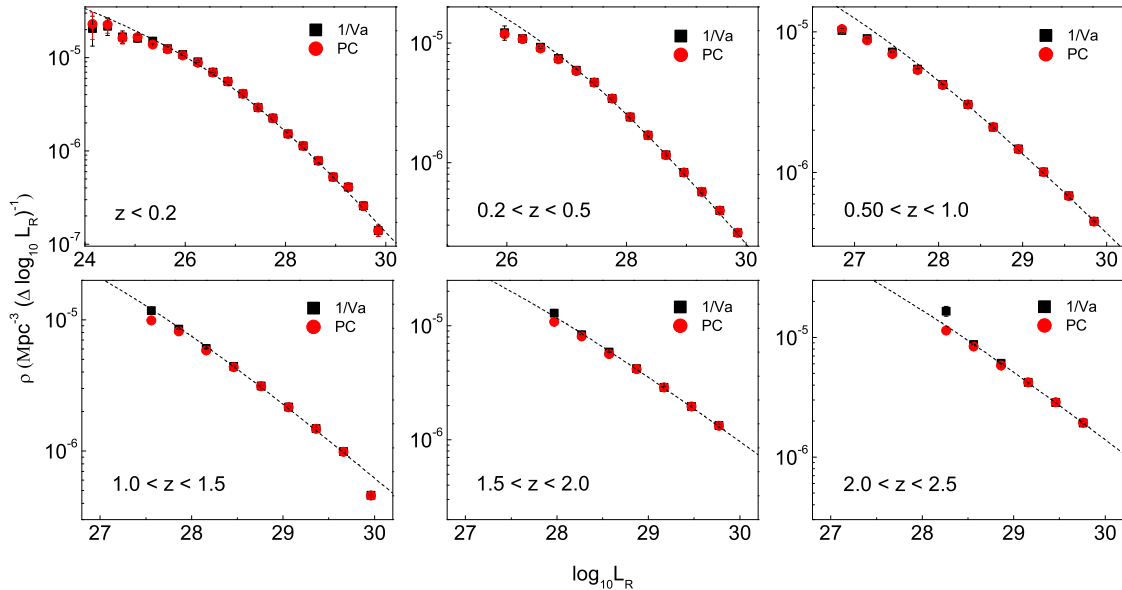


Fig. 11 Binned luminosity functions of simulated samples of objects using ϕ_{1/V_a} and ϕ_{PC} with the binning chosen according to the rule of thumb suggested in section 2.7. The input model LFs take values of $z = 0.12, 0.35, 0.75, 1.25, 1.75, 2.25$ respectively and are shown as dashed lines.

shift and luminosity intervals determined according to the rule suggested above (Fig. 10 (c) specifically). It is noticed that adopting the rule of thumb indeed improved the binned LFs to some extent, especially for ϕ_{1/V_a} . Obviously, ϕ_{1/V_a} is more sensitive to how the intervals are chosen than ϕ_{PC} . Page & Carrera (2000) noticed that for objects close to the flux limit ϕ_{1/V_a} nearly always to be too small. We believe this is due to the arbitrary choosing of redshift and luminosity intervals. If the intervals are chosen appropriately, ϕ_{1/V_a} is only slightly larger than ϕ_{PC} at the faint end of LFs. And it is hard to say the estimate of PC method is markedly better than the $1/V_a$ method. In this sense, the improvement of the PC method over the $1/V_a$ method is probably slight.

3 Non-parametric Methods

A non-parametric method is necessary when investigating the LFs, as it constructs the LFs directly from the data and makes no assumptions about the form of the LFs. Examples of non-parametric methods include the classical $\Phi = N/V$ method (Christensen 1975), the ϕ/Φ method (Turner 1979), the Step-Wise Max Likelihood method (Efsthathiou et al. 1988) and the C^- method (Lynden-Bell 1971), as well as the $1/V_a$ and PC methods discussed here.

The C^- method (also see Willmer 1997; Fan et al. 2001; Choloniewski 1987) is believed to have the advantage over the $1/V_a$ method as it does not require any binning of data, and rests on a strong mathematical foundation (see Woodroffe 1985). The key assumption in the C^- method is that the luminosities and redshifts are independent, but researches on the LFs of AGNs have indicated that there are both luminosity and density evolutions and the independence assumption is incorrect (e.g., Pei 1995; Willott et al. 2001). Some authors (Efron & Petrosian 1992; Maloney & Petrosian 1999) developed the C^- method to remove the correlation of luminosities and redshifts by defining new independent variables (say $L' \equiv L/g_k(z)$ and z , where the function $g_k(z)$ describes the luminosity evolution). Then the C^- method can be used for the (L', z) data. In this sense, the improved C^- method is no longer a non-parametric method as $g_k(z)$ is parameter dependent. Usually, a simple form $g_k(z) = (1+z)^k$ is used, where k is a free parameter. Then a so-called test statistic τ is performed to determine k by making $\tau(k) = 0$ (see Maloney & Petrosian 1999; Singal et al. 2011). In most cases, the $(1+z)^k$ form is too simplistic. E.g., Pei (1995) used a Gaussian form and two free parameters were introduced. Consequently, the unknown luminosity evolution $g_k(z)$ restricts the C^- method.

Notably, in recent years more rigorous approaches, although not all of which are non-parametric, have been

proposed. E.g., Schafer (2007) developed a powerful semi-parametric approach which is built on a nonparametric extension of maximum likelihood called local likelihood modeling. It is expected that a new method needs time to be recognized and in widespread use. Besides, when combining multiple samples to estimate the LFs, the truncation boundary (as discussed in Schafer 2007) of data in the $L - z$ plane is further complicated. The new non-parametric methods are also supposed to deal with this challenge.

4 Summary

The classical $1/V_a$ and PC methods of constructing binned luminosity functions (LFs) are revisited and compared by graphical analysis. The two methods give different estimate of ϕ for the bins which are crossed by the flux limit curves $L = L_{lim}(z)$. Using the combined sample established by Yuan & Wang (2012), we show that ϕ_{1/V_a} trends to give a smaller estimate than ϕ_{PC} at the faint end of LFs, while it gives a larger estimate in the middle of the LFs.

Using a combined sample simulated by a Monte Carlo method, the estimate of two methods are compared with the input model LFs. The two methods give identical and ideal estimate for the high luminosity points of each redshift interval. However, for the low luminosity bins of all the redshift intervals both methods give smaller estimate than the input model. We conclude that once the LF is evolving with redshift, the classical binned methods will unlikely give an ideal estimate over the total luminosity range.

Page & Carrera (2000) noticed that for objects close to the flux limit ϕ_{1/V_a} nearly always to be too small. We believe this is due to the arbitrary choosing of redshift and luminosity intervals. We noticed that ϕ_{1/V_a} is more sensitive to how the binning are chosen than ϕ_{PC} . We suggest a new binning method, which can improve the LFs produced by the $1/V_a$ method significantly, and also improve the LFs produced by the PC methods. Our simulations show that after adopting this new binning, both the $1/V_a$ and PC methods have comparable results.

Acknowledgments

We are grateful to the referee for very useful comments that improved this paper. We acknowledge the financial supports from the National Natural Science Foundation of China 11133006, 11163006, 11173054, the National Basic Research Program of China (973 Program 2009CB824800), and the Policy Research Program of Chinese Academy of Sciences (KJ CX2-YW-T24).

References

- Avni, Y., & Bahcall, J. N. 1980, *Astrophys. J.*, 235, 694
 Best, P. N., Röttgering, H. J. A., & Lehnert, M. D. 1999, *Mon. Not. R. Astron. Soc.*, 310, 223
 Burgess, A. M., & Hunstead, R. W. 2006, *Astron. J.*, 131, 100
 Cara, M., & Lister, M. L. 2008, *Astrophys. J.*, 686, 148
 Choloniewski, J. 1987, *Mon. Not. R. Astron. Soc.*, 226, 273
 Christensen, C. G. 1975, *Astron. J.*, 80, 282
 Christlein, D., Gawiser, E., Marchesini, D., & Padilla, N. 2009, *Mon. Not. R. Astron. Soc.*, 400, 429
 Civano, F., Brusa, M., Comastri, A., et al. 2011, *Astrophys. J.*, 741, 91
 Eales, S. 1993, *Astrophys. J.*, 404, 51
 Efron, B., & Petrosian, V. 1992, *Astrophys. J.*, 399, 345
 Efsthathiou, G., Ellis, R. S., & Peterson, B. A. 1988, *Mon. Not. R. Astron. Soc.*, 232, 431
 Ellis, R. S., Colless, M., Broadhurst, T., Heyl, J., & Glazebrook, K. 1996, *Mon. Not. R. Astron. Soc.*, 280, 235
 Fan, X., Strauss, M. A., Schneider, D. P., et al. 2001, *Astron. J.*, 121, 54
 Hiroi, K., Ueda, Y., Akiyama, M., & Watson, M. G. 2012, *Astrophys. J.*, 758, 49
 Johnston, R. 2011, *Astron. Astrophys. Rev.*, 19, 41
 Johnston, R., Teodoro, L., & Hendry, M. 2012, *Mon. Not. R. Astron. Soc.*, 421, 270
 Kelly, B. C., Fan, X., & Vestergaard, M. 2008, *Astrophys. J.*, 682, 874
 Laing, R. A., Riley, J. M., & Longair, M. S. 1983, *Mon. Not. R. Astron. Soc.*, 204, 151
 Lynden-Bell, D. 1971, *Mon. Not. R. Astron. Soc.*, 155, 95
 Maloney, A., & Petrosian, V. 1999, *Astrophys. J.*, 518, 32
 Mao, M. Y., Sharp, R., Norris, R. P., et al. 2012, *Mon. Not. R. Astron. Soc.*, 426, 3334
 Marchã, M. J. M., & Caccianiga, A. 2013, *Mon. Not. R. Astron. Soc.*, 709
 Marchesini, D., Stefanon, M., Brammer, G. B., & Whitaker, K. E. 2012, *Astrophys. J.*, 748, 126
 Marshall, H. L. 1985, *Astrophys. J.*, 299, 109
 McAlpine, K., & Jarvis, M. J. 2011, *Mon. Not. R. Astron. Soc.*, 413, 1054
 McCarthy, P. J., Kapahi, V. K., van Breugel, W., et al. 1996, *Astrophys. J. Suppl. Ser.*, 107, 19
 Padovani, P., Miller, N., Kellermann, K. I., et al. 2011, *Astrophys. J.*, 740, 20
 Page, M. J., & Carrera, F. J. 2000, *Mon. Not. R. Astron. Soc.*, 311, 433
 Patel, H., Clements, D. L., Vaccari, M., et al. 2012, *Mon. Not. R. Astron. Soc.*, 62
 Pei, Y. C. 1995, *Astrophys. J.*, 438, 623
 Schafer, C. M. 2007, *Astrophys. J.*, 661, 703
 Schmidt, M. 1968, *Astrophys. J.*, 151, 393
 Singal, J., Petrosian, V., Lawrence, A., & Stawarz, L. 2011, *Astrophys. J.*, 743, 104
 Takeuchi, T. T. 2010, *Mon. Not. R. Astron. Soc.*, 406, 1830
 Turner, E. L. 1979, *Astrophys. J.*, 231, 645
 Tzanavaris, P., & Georgantopoulos, I. 2008, *Astron. Astrophys.*, 480, 663
 Willmer, C. N. A. 1997, *Astron. J.*, 114, 898
 Willott, C. J., Rawlings, S., Blundell, K. M., Lacy, M., & Eales, S. A. 2001, *Mon. Not. R. Astron. Soc.*, 322, 536
 Woodroffe, M. 1985, *Ann Stat.*, 13, 163
 Yenko, B., Barger, A. J., Trouille, L., & Winter, L. M. 2009, *Astrophys. J.*, 698, 380
 Yuan, Z., & Wang, J. 2012, *Astrophys. J.*, 744, 84